

HIGH-RESOLUTION [Ne II] OBSERVATIONS OF THE IONIZED FILAMENTS IN THE GALACTIC CENTER

E. SERABYN¹

Max-Planck-Institut für Radioastronomie, Bonn

J. H. LACY¹

Department of Astronomy, University of Texas, Austin

C. H. TOWNES¹

Department of Physics, University of California, Berkeley

AND

R. BHARAT

Rockwell International Science Center, Anaheim

Received 1987 June 12; accepted 1987 August 28

ABSTRACT

The [Ne II] 12.8 μm emission from the central 10" of the Galaxy has been observed with 1".5 resolution. The broad lines previously observed in this region have been resolved into separate features associated with the filaments and knots of radio continuum emission present. Along the filaments, the radial velocity varies rapidly and continuously with position, with gradients of up to 30 $\text{km s}^{-1} \text{arcsec}^{-1}$ observed. The emission along the "eastern arm" has also been mapped.

The velocities measured along the filaments are consistent with streams of gas in orbit about the center. These features have been modeled by gravitationally dominated orbits, and satisfactory fits to the data have been obtained. The masses estimated to lie within the orbits suggest the presence of a central mass of $\sim 2.5 \times 10^6 M_{\odot}$. Possible objections to this simple model are explored, as are the implications for the stellar cluster at the Galactic center. In particular, if a point mass as large as is indicated by the orbits is present, the stellar cluster within the inner few parsecs can have various density distributions; for example, it may vary approximately as $r^{-1.7}$ at all radii, or the cluster may correspond to an isothermal King model with a core radius of $\sim 1 \text{ pc}$.

Subject headings: galaxies: The Galaxy — galaxies: nuclei — infrared: spectra

I. INTRODUCTION

The kinematics of the ionized gas within the central few parsecs of our Galaxy have been investigated with the [Ne II] 12.8 μm line (Wollman *et al.* 1976, 1977; Lacy *et al.* 1979, 1980; Serabyn 1984; and Serabyn and Lacy 1985, hereafter Paper I), the H 76 α line (van Gorkom *et al.* 1983), and the H 66 α line (Mezger and Wink 1986). The high-resolution H 76 α and [Ne II] observations have shown that at least two of the ionized filaments seen in radio continuum maps of the region (Brown and Johnston 1983; Ekers *et al.* 1983; Lo and Claussen 1983; Lo 1986; Morris and Yusef-Zadeh 1987; Ishiguro *et al.* 1987; Wright *et al.* 1987) are apparently in orbit about the center. One of these filaments (the "western arc") traces out the ionized inner edge of a more extensive rotating molecular ring or disk (Becklin, Gatley, and Werner 1982; Genzel *et al.* 1985; Liszt, Burton, and van der Hulst 1985; Harris *et al.* 1985; Sandqvist, Wooten, and Loren 1985; Gatley *et al.* 1986; Lugten *et al.* 1986; Serabyn *et al.* 1986; Güsten *et al.* 1987), while the second filament (the northern arm) is apparently located interior to this ring, closer to the Galactic center, and follows a more eccentric orbit (Paper I). The velocity variations along these two features have been used to estimate the mass enclosed within their orbital radii, giving evidence for a central concentration of mass.

In the observations of Paper I, not all of the ionized gas in Sgr A was mapped. In particular, the radio continuum filament east of the center, as well as the central 10" diameter region were not mapped, since earlier observations had covered these regions fairly well (Lacy *et al.* 1980). These earlier [Ne II] observations showed broad emission in the central few arcsec region (FWHP $\sim 200 \text{ km s}^{-1}$), with velocities up to $\pm 260 \text{ km s}^{-1}$ present. Here "the center" loosely refers to the few arcsec region surrounding the radio point source Sgr A* (Lo *et al.* 1981, 1985; Backer and Sramek 1982, 1987) and the 2 μm source IRS 16 (Becklin and Neugebauer 1975; Allen and Sanders 1986; Forrest, Pipher, and Stein 1986).

Since recent modifications to the Berkeley Fabry-Perot interferometer have made possible observations with significantly improved spatial and spectral resolutions, new observations of the [Ne II] emission from the central region have been made with a 1".5 beam. These observations have successfully resolved the broad lines previously seen in the region. The emission along the eastern filament has also been measured. The spectra are presented in § II, and the velocity components and their variation with position are discussed in § III. In § IV, general models for the ionized filaments are discussed, and in § V the observed features are modeled as flows of gas. Finally, in § VI, the mass distribution implied by the modeling is discussed.

II. OBSERVATIONS

The observations were made in 1984 May and 1985 June/July with the NASA 3 m IRTF, using the Fabry-Perot grating

¹ Visiting Astronomer at the Infrared Telescope Facility, which is operated by the University of Hawaii under contract with the National Aeronautics and Space Administration.

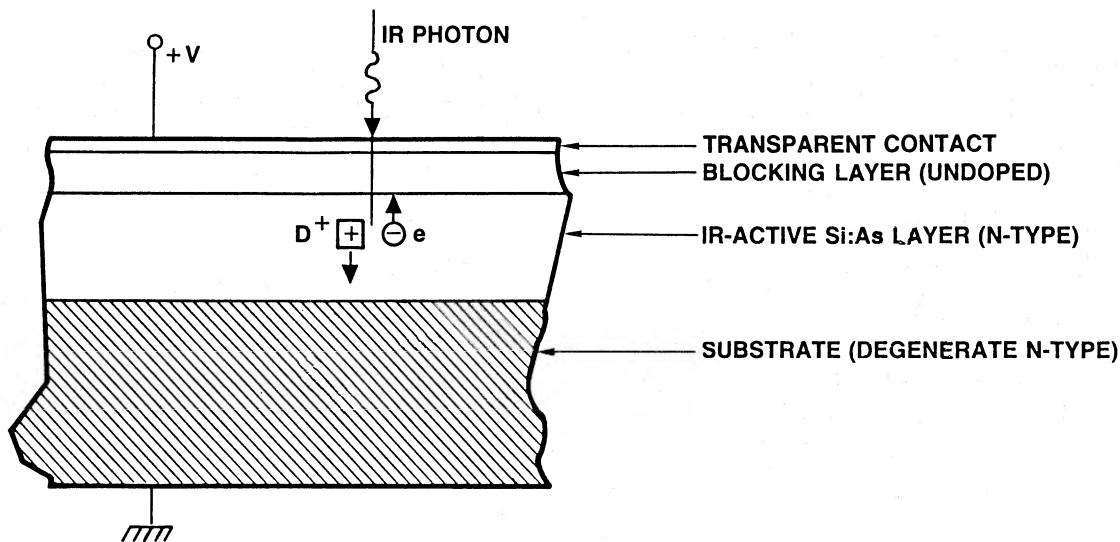


FIG. 1.—Schematic cross-sectional view of a blocked impurity band detector

spectrometer described by Lacy (1979) and Serabyn (1984). Beam sizes of $3''$ and $1''.5$, and a spectral resolution of 25 km s^{-1} were used. A new high quantum efficiency Si:As blocked-impurity-band (BIB) detector made by the Rockwell Science Center was used for these observations. The previous Si:As photoconductor was relatively insensitive when small beam sizes were used, since a small beam only partially illuminated the area between its electrodes, resulting in the unilluminated portions having a resistivity too high to pass current efficiently. Because the BIB detector has a front surface electrode, the responsivity of this detector is essentially independent

of the fraction of the detector illuminated. This allows the same detector to be used for both large and small beam observations with good sensitivity. The resulting system NEP with a $1''.5$ beam and 25 km s^{-1} resolution was $\sim 3 \times 10^{-15} \text{ W Hz}^{-1/2}$.

Since the BIB detector (Petroff and Stapelbroek 1980) is quite new to astronomy, and has advantages as indicated above, a brief description of it follows. In this type of detector, infrared radiation passes through a transparent front surface electrode and a thin undoped silicon layer to the IR-sensitive silicon layer which is heavily doped with arsenic (Fig. 1). The

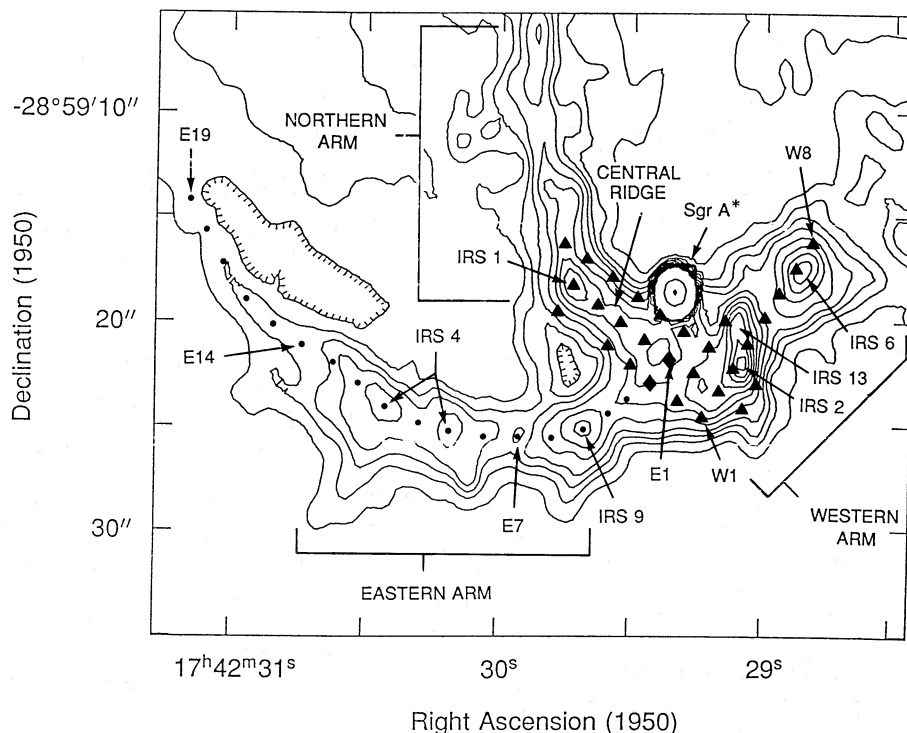


FIG. 2.—The positions at which $[\text{Ne II}]$ spectra were observed, superposed on the 5 GHz map of Lo and Claussen (1983). The points and triangles indicate positions measured with $3''$ and $1''.5$ beams, respectively. The diamonds indicate positions observed with both beams.

undoped (or blocking) layer and the arsenic doped silicon (Si:As) layer are epitaxially grown on a degenerately doped n -type Si substrate which acts as the back electrode. The concentration of As in the IR-sensitive layer is high enough to form an impurity band which allows rapid transport of ionized donor charge by means of hopping conduction in the presence of an electric field. Thus, the electron (e) and ionized donor (D^+) which are created in the IR-sensitive layer by an incident photon can both contribute to the photocurrent when a bias voltage is applied to the detector electrodes. With the bias polarity shown in the figure, no charge injection from the front electrode into the IR-sensitive layer can take place, since the undoped layer lacks an impurity band and thus blocks the corresponding dark current flow associated with hopping conductivity. Because the IR-sensitive layer is heavily doped, good quantum efficiency can be obtained in a relatively thin (about 10 to 20 micrometers) layer, especially at $\lambda > 10 \mu\text{m}$. Since there is virtually no recombination of electrons and ionized donors at low photon flux densities (Petroff and Stapelbroek 1980), the BIB detector has an inherently lower background limited noise [by a factor of $(2)^{1/2}$] than an Si:As photoconductive detector of equivalent quantum efficiency.

The positions at which spectra were measured are shown in Figure 2, superposed on the arcsecond resolution 5 GHz radio continuum map of the central portion of Sgr A West of Lo and Claussen (1983). Pointing was determined by peaking up on the [Ne II] emission from IRS 1 (Fig. 2). Since the [Ne II] line arises in ionized regions, the peaking-up procedure probably aligned our reference position with the 5 GHz emission peak at $\alpha = 17^{\text{h}}42^{\text{m}}29^{\text{s}}.7$, $\delta = -28^{\circ}59'18''.3$, which likely corresponds to IRS 1W, one of the components of IRS 1 (Storey and Allen 1983). With our beam size, the distinction between these locations is not important, and this peak will be referred to simply as IRS 1. In the case of the $1''.5$ observations, the pointing was checked at least after every second spectrum. During the integration times of 2.5 to 10 minutes, the tracking was usually stable to better than an arcsecond, and relative pointing should be about this accurate.

Along the eastern arm, a series of 19 positions were observed with a $3''$ beam. The spacing between positions was $\sim 1''.4$ for positions E1 to E5 and $\sim 1''.8$ for E5 to E19. Figure 3 shows the spectra observed at these positions, arranged according to their order on the sky. For reference, the spectra measured on the radio peaks are labeled by their corresponding IRS numbers (see, e.g., Gezari *et al.* 1985).

Spectra of the central region with the $1''.5$ aperture were obtained on two nights of sub-arcsecond seeing, after careful focusing of the telescope. Drift scans through α Sco indicated that seeing and diffraction broadened the beam only slightly, to $\sim 1''.8$. The positions observed with this aperture are indicated in Figure 2 by the triangles (and diamonds) on the tilted square grid. The spacing of the grid is $1''.4$, and its orientation is such that one of its axes lies along the ridge of radio continuum emission which extends approximately southwestward (at position angle 235°) from IRS 1. This ridge will be referred to as the "central ridge." The observed positions lie essentially along three strips parallel to the central ridge, and one perpendicular strip which passes through IRS 2 and 6 (hereafter the "western strip").

The spectra observed along the three NE-SW strips, as well as at two neighboring positions, are shown in Figure 4, with each approximately NE-SW sequence of spectra presented vertically. The spectra along the western strip are shown in

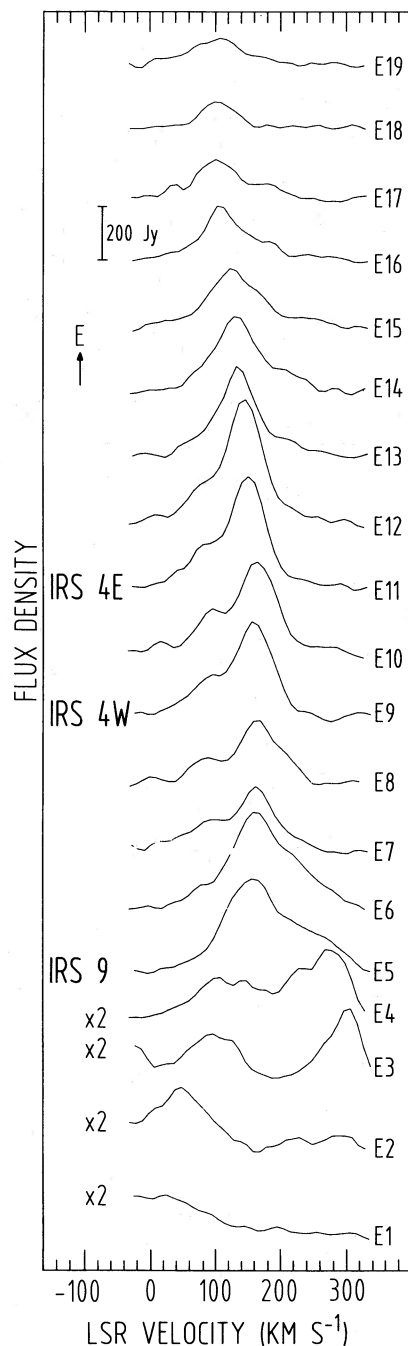


FIG. 3.—Sequence of 19 spectra observed at the positions along the eastern arm given in Fig. 2. The spatial and spectral resolutions are $3''$ and 25 km s^{-1} , respectively. Moving up the figure corresponds to moving eastward along the arm.

Figure 5. For reference, the spectra at IRS 1, 2, and 6 are labeled on these figures. The emission along the central ridge and the western strip are also presented in the form of position-velocity plots in Figures 6 and 7, respectively.

Intensity calibration is relative to α Sco, for which a flux density of 1800 Jy is assumed. Line intensities are accurate to $\pm 30\%$. Frequency calibration was determined by means of a sample cell containing NH_3 and is accurate to $\pm 4 \text{ km s}^{-1}$. All velocities are relative to the LSR. Because the total scan of the Fabry-Perot is limited to ~ 14 resolution elements ($\sim 360 \text{ km}$

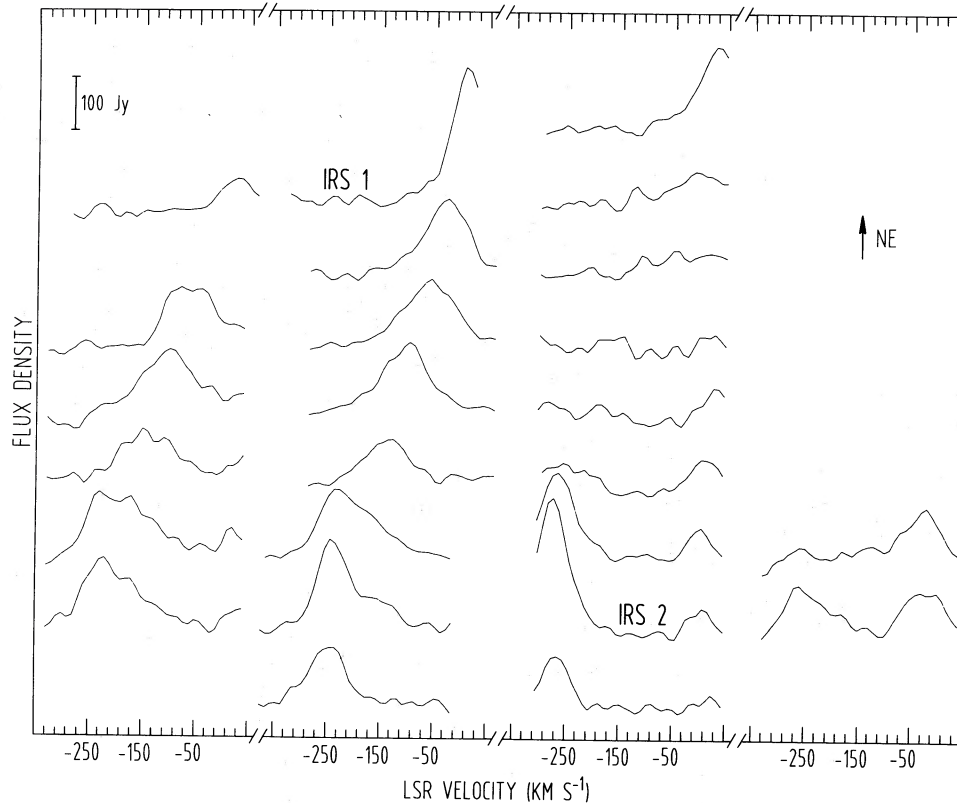


FIG. 4.—Spectra measured on the grid of triangles in the central region of the map in Fig. 2. The spatial and spectral resolutions are $1''.5$ and 25 km s^{-1} , respectively. The orientation of the spectra is such that the \sim NE-SW strips of spectra are presented vertically.

s^{-1}), the velocity interval covered was not extensive enough to encompass all of the emission at all locations. However, since the observations of Lacy *et al.* (1980) show blueshifted emission mainly west of IRS 1, and exclusively redshifted emission on the eastern arm, it was possible to match the velocity range scanned with the velocities present by scanning through redshifted velocities along the eastern arm, and blueshifted velocities in the central region.

III. RESULTS

a) The Eastern Arm

The velocities observed along the eastern arm (Fig. 3) agree well with those determined by Lacy *et al.* (1980) and van Gorkom, Schwarz, and Bregman (1983), but additional detail is evident. The primary result is that the velocity of the main emission peak varies quite regularly with position, increasing from $v_{\text{LSR}} \approx 100 \text{ km s}^{-1}$ at the easternmost position (E19) to a peak of $\sim 165 \text{ km s}^{-1}$ at E10 through E7, and then decreasing slightly by position E5 (IRS 9). This decrease in velocity may continue all the way to E1, as weak emission is present between E4 and E1, with a velocity which decreases from $\sim 110 \text{ km s}^{-1}$ at E4 to $\sim 0 \text{ km s}^{-1}$ at E1. Because of its weakness, it is not certain that this velocity feature is a continuation of the eastern arm, but the continuity of the velocities suggests that it is. The suggested falloff of velocity to a zero crossing near the center implies that the eastern arm may be quite similar to the northern arm (Paper I) and may also represent an orbit about the center.

A second emission component present in the spectra between positions E3 and E6 is due to the “ $+260 \text{ km s}^{-1}$

cloud” (Lacy *et al.* 1980). The velocity of this component is highest (300 km s^{-1}) at E3 and decreases away from the center, to $\sim 230 \text{ km s}^{-1}$ at E6, where this component is seen as a red wing on the main 160 km s^{-1} component. Because of the small spatial extent of this high-velocity emission, we shall continue to refer to this gas as the “ 260 km s^{-1} cloud,” even though its velocity varies with position. Since the main emission peak at 160 km s^{-1} does not show a clear spatial velocity shift in the direction which would indicate a connection with the 260 km s^{-1} cloud, it seems unlikely that these two velocity components are related. However, because of the overlap of the lines, such a connection cannot be entirely ruled out. Also present in the spectra is relatively constant velocity emission at $\sim 80 \text{ km s}^{-1}$ near IRS 4. Because spatially extended gas near 100 km s^{-1} is present in this region (Serabyn 1984), this gas is probably not related to the filamentary eastern arm.

b) The Central Region

Earlier [Ne II] observations of the central region with spectral and spatial resolutions of 77 km s^{-1} and $3''.5$, respectively, showed very broad lines ($\geq 200 \text{ km s}^{-1}$ FWHM) and multiple velocity components (Lacy *et al.* 1980). In contrast, many of the spectra in Figures 4 and 5 show only a single velocity component of width $50\text{--}100 \text{ km s}^{-1}$, and several spectra show little or no emission. The differences with the earlier data can be accounted for primarily by the higher spatial resolution of these observations, which has allowed different velocity features to be spatially separated. A careful comparison of Figures 4 and 5 with the earlier data indicates that all of the velocity

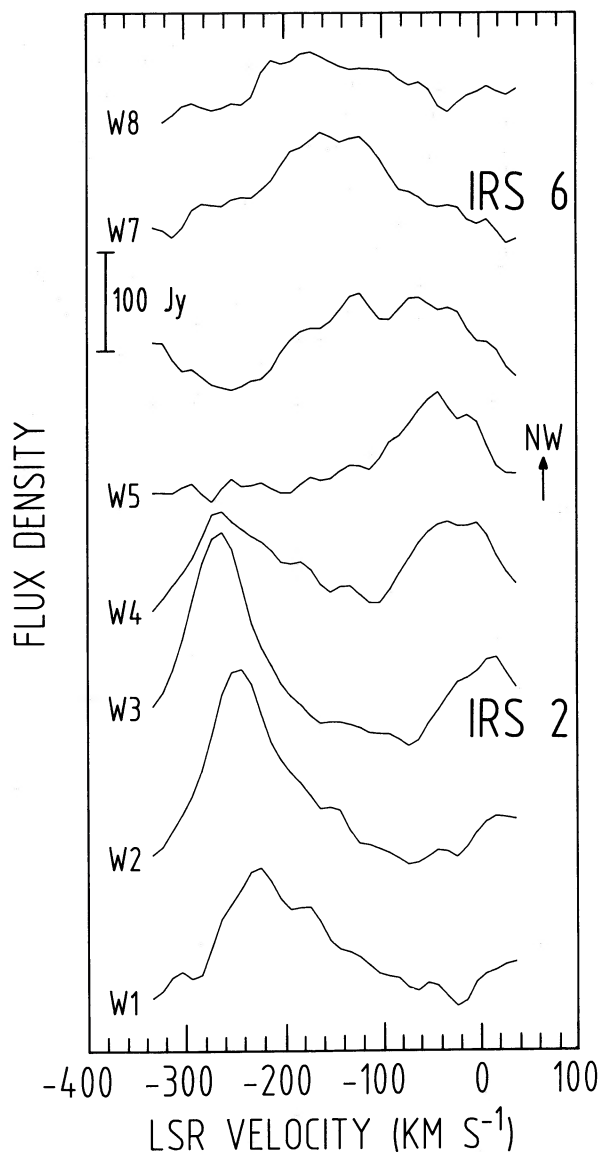


FIG. 5.—Spectra measured along the \sim NW-SE “western arm” shown in Fig. 2. The spatial and spectral resolutions are as in Fig. 4.

components present in the larger beams are accounted for. However, remarkable new detail is evident.

The most striking new aspect is that along the central ridge (Figs. 4 and 6), only a single velocity feature is present, with a velocity which varies very rapidly and regularly with position. Beginning at ~ 0 km s^{-1} near IRS 1, the velocity varies smoothly to ~ -170 km s^{-1} only 6".5 to the SW (with a velocity gradient of 25 to 30 $\text{km s}^{-1} \text{arcsec}^{-1}$), and then takes a somewhat larger jump (just SW of E1) to a final velocity of ~ -240 km s^{-1} near IRS 2. Although the spectra along the central ridge suggest that the velocity centroid jumps slightly to its final value of -240 km s^{-1} , the position-velocity plot of Figure 6 suggests a smoother continuation (as do the line wings in the spectra), implying that the jump may be caused by clumpiness in the gas distribution. In either case, the velocities finally blend into the high negative velocity emission region known as the “ -260 km s^{-1} cloud” (Lacy *et al.* 1980) near

IRS 2. (This same velocity pattern has recently been seen by Lacy, Lester, and Arens 1987).

The continuous large velocity gradient emission seen along the central ridge most probably arises in that radio continuum filament, because corresponding emission is absent in the parallel strip of spectra to the NW. In addition, low spectral resolution Br α mapping shows the thermal line emitting region to coincide with the central ridge (Forrest *et al.* 1987). The uniformity of the velocity gradient along the central ridge, and the fact that it apparently extends far enough to encompass the -260 km s^{-1} emission near IRS 2, suggests strongly that the “ -260 km s^{-1} cloud” is part of the same continuous gas feature, rather than being an isolated entity. If so, all of the emission seen between IRS 1 and 2 can apparently be accounted for by this one gas filament. The high brightness near IRS 2 and the lack of emission farther to the west could then result from the gas filament being nearly tangential to the line of sight at this point.

On the radio continuum map, the central ridge seems to be the extension of the northern arm into the central region, although there is a distinct difference in direction between the central ridge and the northern arm. The observed velocities support this idea, since the radial velocity varies monotonically along the combined feature, from ~ 140 km s^{-1} north of IRS 1, to 0 km s^{-1} near IRS 1 (Paper I), to more negative velocities along the central ridge, and finally to -260 km s^{-1} near IRS 2. Thus, the northern arm, the central ridge, and the -260 km s^{-1} cloud appear to be part of one coherent gas feature (referred to below as the “extended northern arm”; the name “northern arm” will be reserved for the section north of IRS 1). Since the velocity along the extended northern arm crosses 0 km s^{-1} near the Galactic center, gas orbiting about the center is suggested.

The only additional velocity component present in the region mapped in Figure 4 is emission at ~ 0 km s^{-1} located somewhat NW of IRS 2. This velocity component can best be investigated with the aid of the position-velocity diagram along the western strip (Fig. 7). The most prominent feature on this plot is the aforementioned -260 km s^{-1} emission near IRS 2, which is seen to become more blueshifted toward the northwest. The 0 km s^{-1} emission near IRS 2 also becomes more blueshifted toward the northwest, and subsumes both the 0 and -60 km s^{-1} “clouds” of Lacy *et al.* (1980) into a single continuous feature. This feature may continue even further northwestward, with a steepening velocity gradient, to connect to the -150 km s^{-1} emission near IRS 6. Because the line broadens near IRS 6, the alternative that an additional velocity feature is present near IRS 6 is also possible. However, given the trend of greater blueshifts toward the northwest, it seems more likely that all of this gas is part of one coherent gas structure. If so, all of the strong blueshifted emission in the central region would be due to only two gas features: the central ridge between IRS 1 and IRS 2, and the feature just discussed along the western strip (approximately between IRS 2 and 6). The latter feature will be referred to as the “western arm.” It is interesting that for this feature also, the velocity crosses zero close to the Galactic center.

Position W6 shows higher velocity emission than has previously been seen in the [Ne II] line, at ~ -350 km s^{-1} (Fig. 5). (Other high velocities have now also been detected by Lacy, Lester and Arons 1987). Because this emission appears in only one position, and falls partially off the end of the scan, its spatial extent is not clear. However, the velocity structure

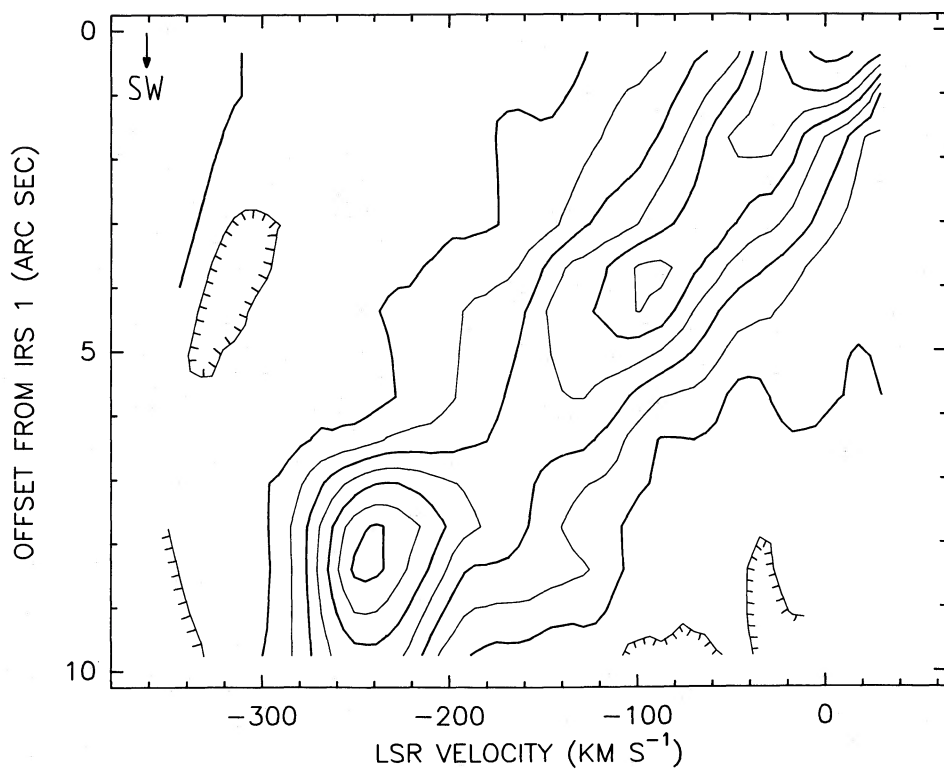


FIG. 6.—Position-velocity diagram for the spectra along the “central ridge” of emission shown in Fig. 2. Moving down in the figure corresponds to moving SW along the ridge. Offsets from IRS 1 are in a direction 235° from north. The contour levels are 20, 40, 60, ... Jy per beam.

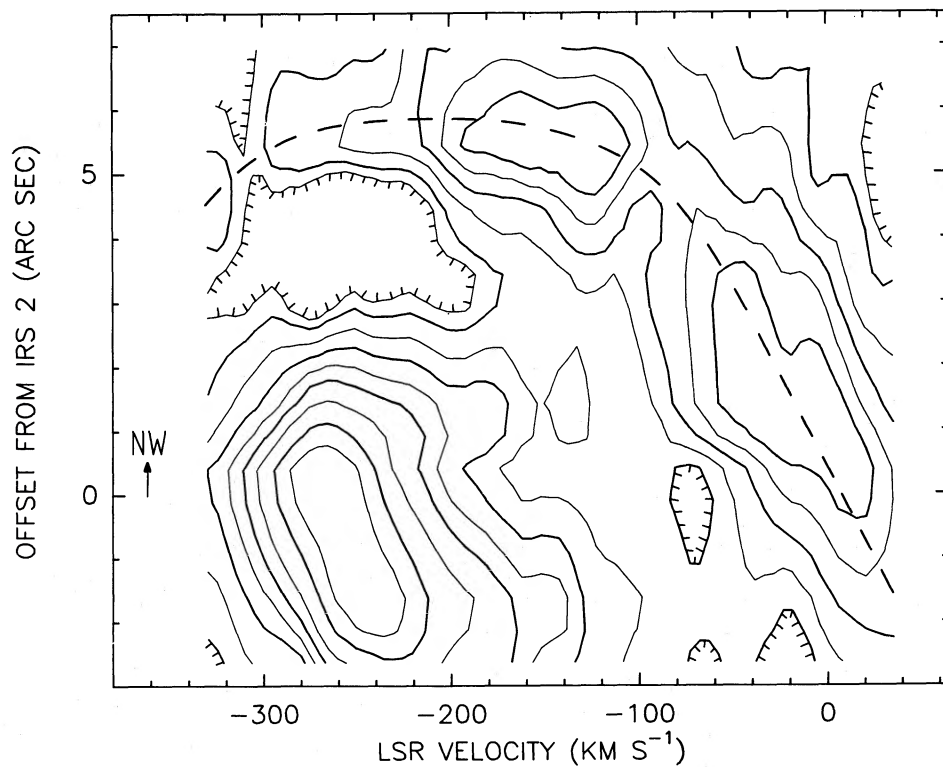


FIG. 7.—Position-velocity diagram for the spectra along as the “western arm” in Fig. 2. Moving up in the figure corresponds to moving approximately NW on the sky (direction 325° from north). The contour levels are 20, 30, 45, 60, 75, 90, 110, 140, 170 Jy per beam.

present in Figure 7 suggests that this gas may be related to the emission near IRS 6, since except for the -260 km s^{-1} emission near IRS 2, all of the emission along the western strip could be connected with the smooth curve shown. Alternatively, the -350 km s^{-1} gas might be related to the -260 km s^{-1} emission near IRS 2.

IV. DISCUSSION

While the first detailed model of the dynamics of the ionized gas in the Galactic center ascribed each velocity feature to an independent gas cloud orbiting about the center (Lacy *et al.* 1980; Lacy, Townes, and Hollenbach 1982), the more recent models have started from the opposite direction, by attempting to account for all of the velocity components present with a minimum number of more extensive gas features (e.g., Brown 1982; Ekers *et al.* 1983; Lo and Claussen 1983; Brown and Liszt 1984; Quinn and Sussman 1985; Serabyn and Lacy 1985; and Heyvaerts, Norman, and Pudritz 1987). Although several of the specific models have been ruled out on the basis of a disparity between the observed and predicted velocities, such as the precessing twin-jet model of Brown (1982) (see Ekers *et al.* 1983 or Lo and Claussen 1983), the "mini-spiral" suggestion of Ekers *et al.* (see Lo and Claussen 1983 or Serabyn and Lacy 1985), and the decaying orbit model of Quinn and Sussman (1985) (see Serabyn 1984), the basic idea of a few extensive gas features is well supported by the observations of van Gorkom, Schwarz, and Bregman (1983), Paper I, and this work.

Of the previous models, the gas measured most closely resembles the suggestion of Lo and Claussen (1983) that the emission in the central region is due to the overlap of three gas features: the northern, eastern, and western arms (the latter should not be confused with the "western arc," the more distant material discussed, for example, in Paper I). Except for the $+260 \text{ km s}^{-1}$ cloud, which does not fit into this pattern, the measured gas does appear to be attributable to three such features. However, the velocities measured along the eastern and western arms conflict with the velocity variation proposed in the infall scenario of Lo and Claussen (1983), in which the Doppler shift along the eastern and western arms was suggested to increase toward the center. In contrast, the blueshift evidently decreases toward the center along the western arm, and the gas with the highest blueshift is associated not with the western arm, but with the extended northern arm. Along the eastern arm, although the velocities do increase toward the center at large distances, they too seem to show a decrease to zero velocity at smaller distances. In addition, the 260 km s^{-1} cloud suggests that at least a fourth velocity feature is present.

In terms of general models, the velocity zero crossings present near the center in the western arc (Paper I) and the extended northern arm, and less clearly in the eastern and western arms, are inconsistent with motion dominated by overall central expansion. Furthermore, outflowing jets from a common source also appear ruled out, because the filaments pass by the center, rather than originating at a common point (Lo and Claussen 1983). On the other hand, both observations are consistent with gas orbiting about the center. Thus, a model in which the ionized filaments represent gas orbiting about the center neatly accounts for most of the ionized gas present within 2 pc of the center, including the centralmost region (roughly between IRS 6 and IRS 9), which is frequently referred to as the "bar." Further support for a common model for all of the gas filaments comes from the similar linewidths

seen in all of the ionized features ($\sim 50 \text{ km s}^{-1}$). Thus, the new kinematic data suggest that the gas along the bar is no different from the other filamentary features, in contrast to the models proposed by Brown and Liszt (1984), Mezger and Wink (1986), and Heyvaerts, Norman, and Pudritz (1987).

The bar does differ from the more distant filaments in Sgr A West in that radio recombination line emission has been detected from all of the ionized filaments in Sgr A except for the bar (van Gorkom, Schwarz, and Bregman 1983). This could be the result of a higher kinetic temperature (van Gorkom, Schwarz, and Bregman 1983; Brown and Liszt 1984) or density (Serabyn 1984) in the bar region and does not imply a different kinematic origin for the bar. In particular, a higher kinetic temperature in the centralmost region would be a natural consequence of an orbit which passes closer to ionizing sources which are centrally located.

We now turn to more specific orbit models. Because the observed velocities do not vary linearly with distance along several of the filaments (Paper I and Fig. 8), orbit models which include radial motion must be considered. Although orbit models can proceed from a variety of assumptions, the simplest are that the orbits are dominated by gravity, and that the gas flow is directed along the filaments. Are these assumptions plausible? Regarding the first assumption, possible non-gravitational forces which might be important include drag produced by an interfilament medium (Quinn and Sussman 1985), buoyant pressure due to a centrally outflowing wind (Hall, Kleinmann, and Scoville 1982; Geballe *et al.* 1984; Krisciunas, Geballe, and Wade 1985; Geballe 1987), and magnetic forces (Aitken *et al.* 1986). The drag suggestion has the difficulty that in order for a drag large enough to significantly affect an orbit in only one pass by the center to be present, the drag medium must be nearly as dense as the filaments themselves (Quinn and Sussman 1985). Observational and theoretical constraints limit the possible interfilament medium to a narrow temperature range: $\sim 10^5$ to a few $\times 10^6 \text{ K}$ (Quinn and Sussman 1985; Genzel and Townes 1987). Such a hot intercloud medium occurs elsewhere in the Galaxy (e.g., McCray and Snow 1979), but has not been detected directly in the Galactic center because of intervening absorption at soft X-ray wavelengths.

A wind of the magnitude inferred from observations of broad H and He emission near IRS 16 could have significant dynamical effects on the filaments. However, the nature of the broad line emitting region is not clear; the most recent observations suggest that the observed broad line region is a shock front wherein an even higher velocity (unobserved) wind is decelerated (Geballe *et al.* 1987). Furthermore, since the observed velocities imply that expansion does not dominate the motion of the filaments, the effect of the proposed wind on the filaments may not be large.

Magnetic effects are also uncertain. Aitken *et al.* (1986) infer, from the presence of aligned grains, a magnetic field of greater than 10 mG oriented along the northern arm. Since the tidal stretching of a cloud of infalling gas would tend to amplify the magnetic field component frozen into the gas which is aligned with the flow, the observed field direction is expected in an infalling streamer. Whether the field has significant dynamical effects is difficult to determine without knowledge of its geometry, but an estimate of its importance can be made by comparing the magnetic and kinetic energy densities. For a density of 10^5 cm^{-3} and a velocity of 150 km s^{-1} (a lower limit to the velocity if the northern arm is in orbit about the

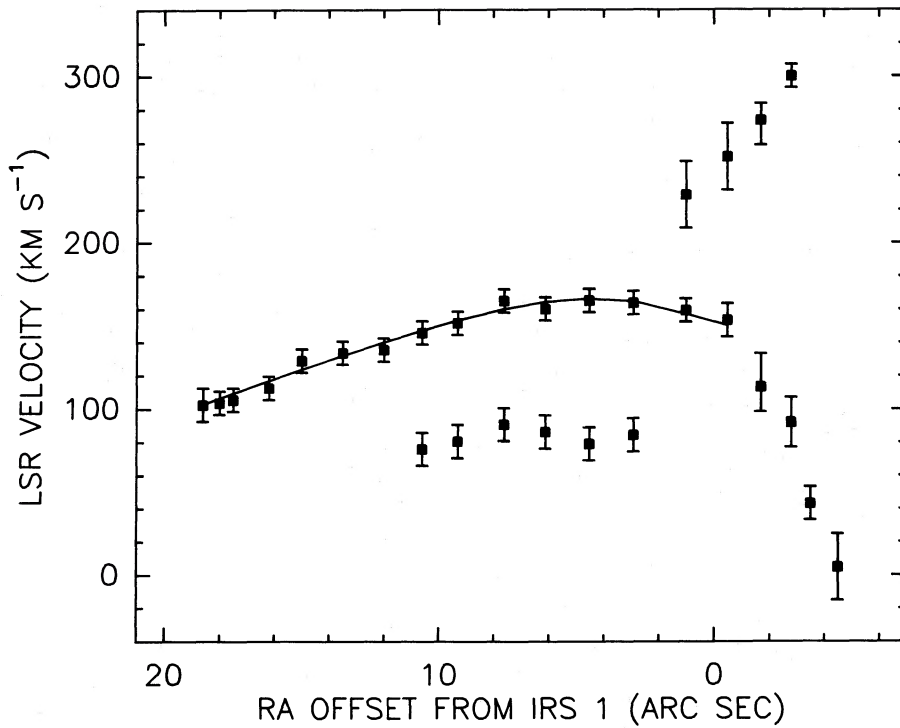


FIG. 8a

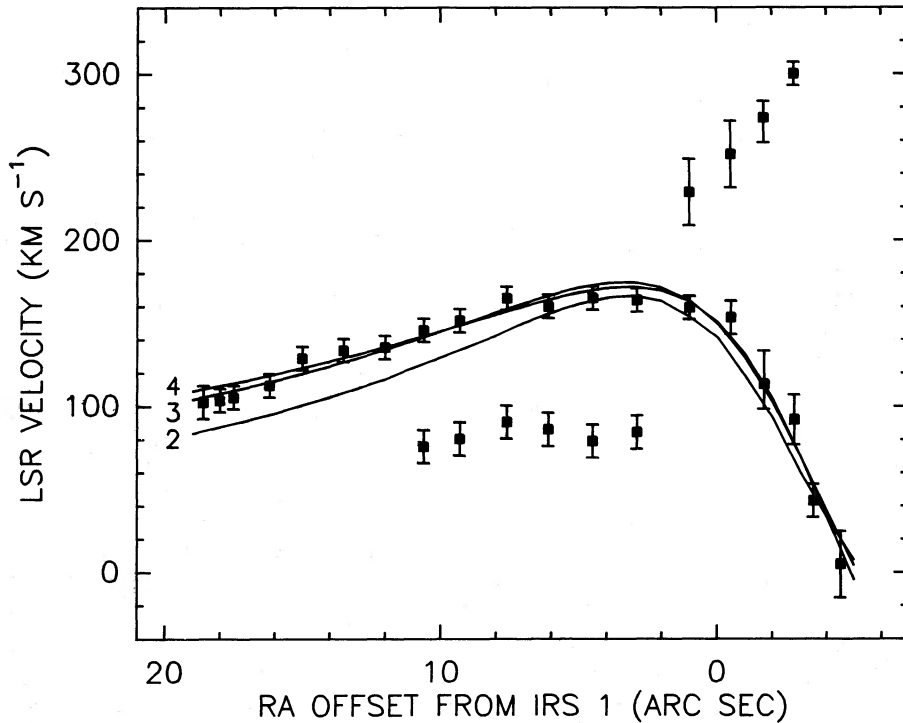


FIG. 8b

FIG. 8.—(a) Best fit to velocities along the eastern arm as a function of right ascension offset from IRS 1. The curve shows a fit to the high-velocity section of the eastern arm produced by an orbit in an r^{-2} stellar cluster with $M_{1.7} = 5 \times 10^6 M_{\odot}$. (b) Same as (a) except that the curves are fits to the entire proposed feature produced by parabolic orbits about a point mass $2''$ E and $2''$ S of Sgr A*. The numbers labeling the curves give the mass of the central object in $10^6 M_{\odot}$. (c) Fits to the position of the eastern arm for parabolic orbits about a point mass of $3 \times 10^6 M_{\odot}$ located at the three positions indicated by the \times , $+$, and \odot (for curves 1, 2, and 3, respectively). The dashed line shows the spatial fit obtained for an orbit in a stellar cluster with $M_{1.7} = 10^7 M_{\odot}$ centered at the $+$ symbol. (d) Best fits to the velocities along the entire eastern arm produced by orbits in stellar clusters with the indicated values of $M_{1.7}$.

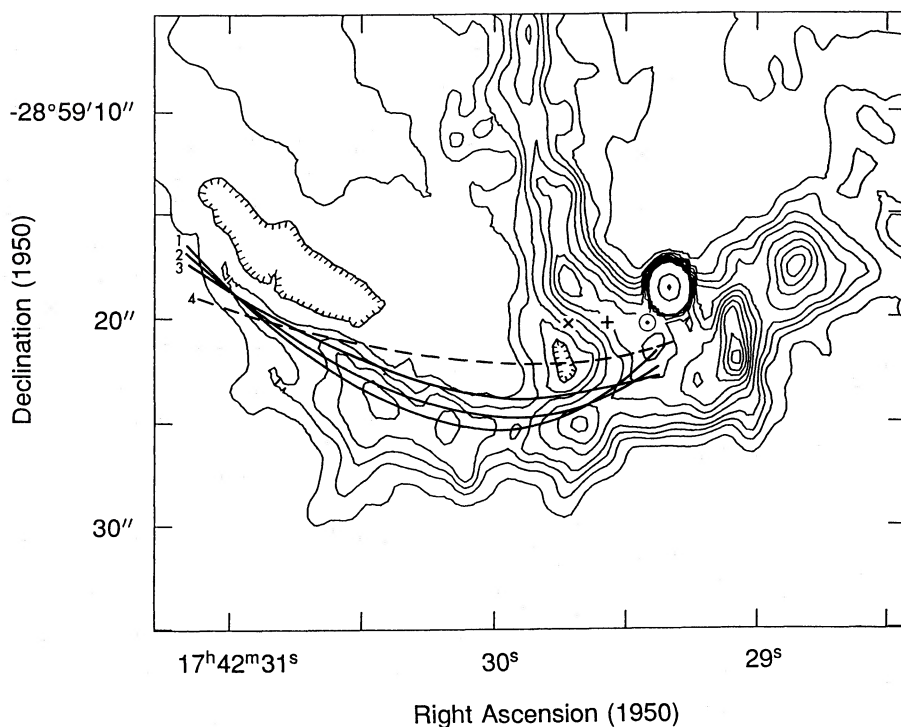


FIG. 8c

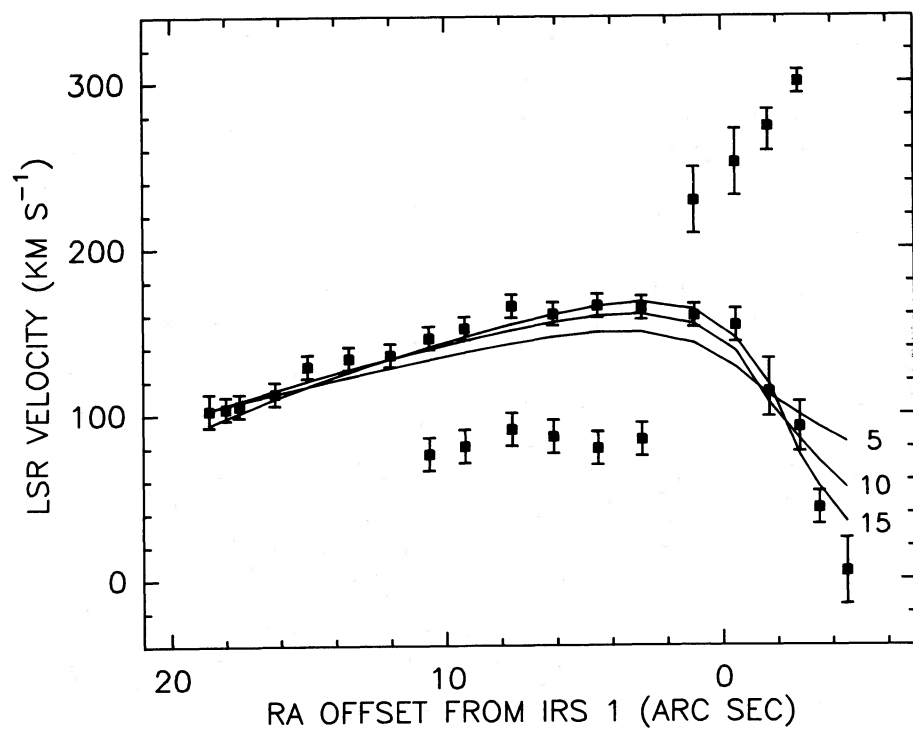


FIG. 8d

center), the kinetic energy density is 2×10^{-5} ergs cm^{-3} . The field energy density, however, is $\sim 4 \times 10^{-6}$ ergs cm^{-3} (Aitken *et al.* 1986). It therefore appears that magnetic forces should not seriously affect the motion of the dense filaments. However, it is possible that the field can cause second-order effects, such as the "braiding" observed (Lo 1986; Morris and Yusef-Zadeh 1987). The field could also serve to confine the gas without directing its motion since the thermal energy density is an order of magnitude below the magnetic energy density, which is itself an order of magnitude less than the kinetic energy density.

There is also the question of whether the gas flows purely along the filaments, or if there is in addition some motion transverse to the filaments. This question is related to that of the origin of the filaments, since the motion of the source of the gas will constrain the subsequent motion. Because a central explosion or expansion is ruled out by the velocity pattern, and a concentration of material into elongated structures by a gravitational (or other, unidentified) instability does not present a convincing possibility, the simplest model for the origin of the inner filaments (i.e., all but the western arc) is that they result from eccentrically orbiting gas clouds, which are tidally stretched as they approach the center. In this case, since low angular momentum is necessary for the gas to be able to approach the center (the rotational velocity at a radius of 10 pc must be less than 15 km s^{-1}), the gas must flow primarily along the filaments, with the trailing part of the gas cloud following essentially the same orbit as the leading part. Such a model still requires an explanation for the origin of the eccentrically orbiting gas. However, there are several molecular clouds near the center which have eccentric motions (e.g., the " 50 km s^{-1} " cloud, and the " -30 km s^{-1} " cloud; Brown and Liszt 1984; Bally *et al.* 1987; Serabyn and Güsten 1987), implying that the general scenario is compatible with the observed environment of the Galactic center. In addition, Yusef-Zadeh and Morris (1987) suggest that several of the filaments in the inner parsec may continue out to much larger radii.

Alternatively, the origin of the filaments might lie in the disk of molecular material which surrounds the center at $r \gtrsim 2$ pc. Supporting this origin is the observation that the more distant ends of the northern and eastern arms are apparently located in gaps in the surrounding molecular disk (Güsten *et al.* 1987). Furthermore, the estimated inclinations of the orbits of the various gas features are similar. However, if the filaments originate in this material, the gas in the disk must lose a significant fraction of its angular momentum. This cannot result from a collision between two clumps in the disk, as suggested by Güsten *et al.* (1987), since essentially all of the disk has high angular momentum in the same direction. Thus such a collision would not change the orbital radius greatly. However, loss of sufficient angular momentum can result from a collision with an external, counterrotating cloud, some of which are seen in the region (e.g., the " 0 km s^{-1} " cloud" at the northern tip of the northern arm; Paper I). Since an external cloud would likely collide with the disk at a stationary point in space, the gas torn off the disk would originate at this stationary point, and so should follow a time-independent path, with little motion transverse to the filament.

Thus, although all other cases cannot be excluded, the simple picture in which the filaments represent eccentric orbits in the central gravitational field does present a viable model. The type of orbit necessary is explored in the following section.

It should be added that although the discussion relating to the origin of the filaments has emphasized orbits which approach the center, some of the filaments could equally well have already gone past the center. However, the case of the northern arm suggests that successive collisions (at its northern end and again at IRS 1; see below) remove angular momentum from the gas, causing it to settle to the center.

V. MODEL CALCULATIONS

Simple gravitationally dominated orbit models for the filaments were investigated for two different central mass distributions: a central point mass, and a spherically symmetric stellar cluster with density, ρ , proportional to $r^{-\alpha}$. Calculations were carried out only for α equal to the isothermal value of 2, which is close to the value of 1.7–1.8 determined for the stellar cluster at the Galactic center (Becklin and Neugebauer 1968; Allen, Hyland and Jones 1983). The possible ellipticity of the stellar cluster has been addressed in Paper I.

Orbits in both mass distributions were calculated and fitted to both the position and velocity of several of the filaments. In Paper I, such orbits gave good fits to the northern arm. Here, orbits of this type are fitted to the eastern arm, the extended northern arm, and the central ridge. The western arm was not fitted because the observations in that area are not extensive enough. The fitting procedure was as in Serabyn (1984). First the path and velocity variation for a given orbit in its plane was calculated. After choosing a location for the center, a least-squares fitting program rotated the orbit in space, to simultaneously fit the observed radial velocities with those calculated, and the position of the filament with the projection onto the sky of the calculated orbit. The relative weighting of the spatial and velocity data is somewhat open and was usually chosen so as to give equal weights to 1" and 10 km s^{-1} accuracy.

In the following, the distance to the Galactic center, R_0 , is assumed to be 10 kpc, to be consistent with Paper I. Both distances and masses scale linearly with the assumed distance to the center, and so decrease by 15% if the IAU recommended value of 8.5 kpc is used. Instead of describing the stellar clusters by their densities, their mass enclosed within 1.7 pc of the center, $M_{1.7}$, will be used, to allow direct comparison with the mass estimated to lie within the near-circular orbit of the western arc at that radius ($4.7 \times 10^6 M_\odot$; Paper I):

a) The Eastern Arm

The line-center velocities of all the spectral components present along the eastern arm, determined from multiple-component Lorentzian fits, are shown plotted versus right ascension in Figure 8a. The continuity of the velocities along the arm and the suggested falloff in velocity close to the center are evident. In addition, the 260 km s^{-1} cloud and the 80 km s^{-1} emission near IRS 4 appear as separate features. Because it is not certain that the gas with velocities between 0 and 120 km s^{-1} in positions E1 to E4 is actually the continuation of the eastern arm, orbits were first fitted to the "high velocity section" (E5 to E19), neglecting the zero-crossing section. Afterward, orbits were fitted to all of E1 to E19. Since the ends of the filament are weak, their precise location is uncertain, and so the spatial fit to the endmost positions should not be considered as very significant.

The high-velocity section was easy to fit with an orbit either about a point mass, or in a stellar cluster, primarily because the velocity varies less than 25% from the mean along this section. The velocity fit for the case of a stellar cluster with $M_{1.7} = 5$

$\times 10^6 M_{\odot}$ (the value determined from the western arc) is shown in Figure 8a. The spatial fit is similarly good. The distance of closest approach of the orbit, r_{\min} , is estimated to be ~ 0.4 pc.

The entire arm can also be fitted. Before discussing specific orbits, the shape of the velocity curve can be used to extract some general information on the type of orbit necessary. Since the velocity drops from near its maximum value to ~ 0 km s $^{-1}$ in only 4" to 5", approximating this section of the orbit near r_{\min} as a circle implies $r_{\min} \sim 0.2$ pc. However, to cover the full extent of the arm, the orbit must extend at least 1 pc from the center, implying a rather elongated orbit ($r_{\max}/r_{\min} > 5$).

Turning to specific orbits, first parabolic orbits were fitted for a number of origin positions near IRS 1 and 16. From this it was determined that the best velocity fits occurred with the origin $\sim 2''$ S and $2''$ W of IRS 1 (with an accuracy of $\sim 3''$). The velocity fits for a central point mass, M , of 4, 3, and $2 \times 10^6 M_{\odot}$ located at this position are shown in Figure 8b. Although $M = 4$ or $3 \times 10^6 M_{\odot}$ allow good fits to the velocities, for $M = 2 \times 10^6 M_{\odot}$, the velocities at the more distant points fall short of the observed velocities. This also occurred for all other trial origins. Thus for parabolic orbits, $M > 2.5 \times 10^6 M_{\odot}$ is necessary to obtain a good fit. The program also fitted r_{\min} and gave a value near 0.2 pc, as expected.

Figure 8c shows the spatial fits for a point mass of $3 \times 10^6 M_{\odot}$ located at three different positions. The spatial fit is seen to improve as the origin is moved eastward, because the orbital plane can then be tipped more out of the line of sight, giving more curvature to the projected orbit. The velocities can nevertheless remain high due to the origin being nearer the filament. For the origin location discussed above, the spatial fit is within 1" of the entire eastern arm, and the inclination of the estimated orbital plane with respect to the line of sight is $\sim 40^{\circ}$ to 50° . Hyperbolic and elliptical orbits about this origin were also fitted and resulted in equally good fits. However, in some cases a somewhat smaller central mass also allowed a good fit, implying that for any Keplerian orbit to fit the arm, $M > 2 \times 10^6 M_{\odot}$ is called for.

Again with the same origin, orbits in a stellar cluster with $\rho \propto r^{-2}$ and $M_{1.7} = 15, 10,$ and $5 \times 10^6 M_{\odot}$ were tried. For each value of $M_{1.7}$, the energy-angular momentum ($E - L$) plane was searched for orbits which fit the data well. It turned out to be very difficult to get a good fit to the position of the filament, because the observed velocities could be reproduced only by having the orbital plane nearly edge-on. This resulted in very straight projected orbits, which lay close to the declination chosen for the center, and which did not match the observed curvature of the arm. Figure 8c shows one example of such a fit.

It was, however, possible to find a localized region in the $E - L$ plane, relatively independent of $M_{1.7}$, which optimized the velocity fits. Figure 8d shows the effect on the velocity fit of reducing $M_{1.7}$, with E and L optimized. The figure indicates that reducing the mass in the cluster makes the fit worse, because the lower masses cannot reproduce the curvature seen in the velocity plot. Thus, for a spherical stellar cluster with $\rho \propto r^{-2}$, $M_{1.7} > 10 \times 10^6 M_{\odot}$ is necessary for a good fit to the entire feature.

To summarize the preceding discussion, the points E5 through E19 can be well fitted either by a central point mass, or by a stellar cluster with $M_{1.7} = 5 \times 10^6 M_{\odot}$. To fit the somewhat more doubtful points E1 to E4 as well, a point mass

greater than $2 \times 10^6 M_{\odot}$ suffices, but a larger stellar cluster, with $M_{1.7} > 10 \times 10^6 M_{\odot}$ would be necessary.

b) The Extended Northern Arm

Since Paper I showed that it is possible to fit orbits of these types to the northern arm, the same was attempted for the extended northern arm. Figure 9 shows a plot of the velocities observed along the extended northern arm versus declination. The data north of IRS 1 are from the 3" observations of Paper I, and south of IRS 1 from this paper. There is approximately a 1" uncertainty in the relative placement of the two data sets. While the data show continuity in velocity between the northern arm and the central ridge, there is a change in slope. In crossing IRS 1, the velocity gradient changes suddenly from 10 km s $^{-1}$ arcsec $^{-1}$ on the northern side, to 25 km s $^{-1}$ arcsec $^{-1}$ to the south. As can be seen in Figure 2, the extended northern arm also abruptly changes its orientation from N-S to NE-SW at IRS 1. Because of these discontinuities, it is unlikely that a single orbit could fit the entire feature.

This was in fact borne out by several trial orbits. Figure 9 shows a typical velocity fit for a parabolic orbit around a $4 \times 10^6 M_{\odot}$ central mass. Although the general form and extent of the velocity curve can be reproduced, the fits overshoot the velocities north of IRS 1 because of the change in slope there. The spatial fits similarly smooth out the sharp bend near IRS 1, either by overshooting or undercutting the corner. All Keplerian orbits and stellar cluster orbits have similar smoothing tendencies. Shifting the relative placement of the 3" and 1.5" data by 1" in any direction did not improve the accuracy of the fits, ruling out pointing as the source of the difficulty. Rather, the difficulty arises in the discontinuities at IRS 1. For this reason it does not seem likely that an alternative type of orbit, such as an inward spiraling orbit (e.g., Quinn and Sussman 1985), would improve matters either. Since the fits are poor, little definite information on the mass distribution is obtained by the addition of this extension to the northern arm.

A possible explanation for the discontinuities in the spatial direction and velocity gradient at IRS 1 is a disruption in the orbit of this gas stream, such as by a collision with another gas cloud. A collision could discontinuously change both the direction of the orbit, as well as the radial velocity gradient, while allowing the gas to follow free-fall paths in between collisions. There actually is a candidate for a partner in such a collision, that being the ridge of emission which extends southward approximately from IRS 1 to IRS 9. Such collisions could provide a mechanism for removing angular momentum from stably orbiting gas, allowing it to fall closer to the center. Alternatively, the discontinuities might reflect a deflection due to magnetic fields.

Since the velocity gradient is continuous south of IRS 1, it is possible that after a disturbance at IRS 1, the gas resumes a normal, but different, orbit. To investigate this possibility, orbits were fitted to only the central ridge section, between IRS 1 and IRS 2. Note that the orbit cannot be circular, unless the origin is near IRS 1. Assuming on the other hand that the origin is at the position of Sgr A*, noncircular orbits result in good fits to both the velocity and position of this filament. Thus, the gas along the central ridge may in fact be following a single undisturbed orbit. Examples of Keplerian orbit fits are shown in Figure 10, superposed on the position-velocity plot of the central ridge. Although the specific fits shown are for para-

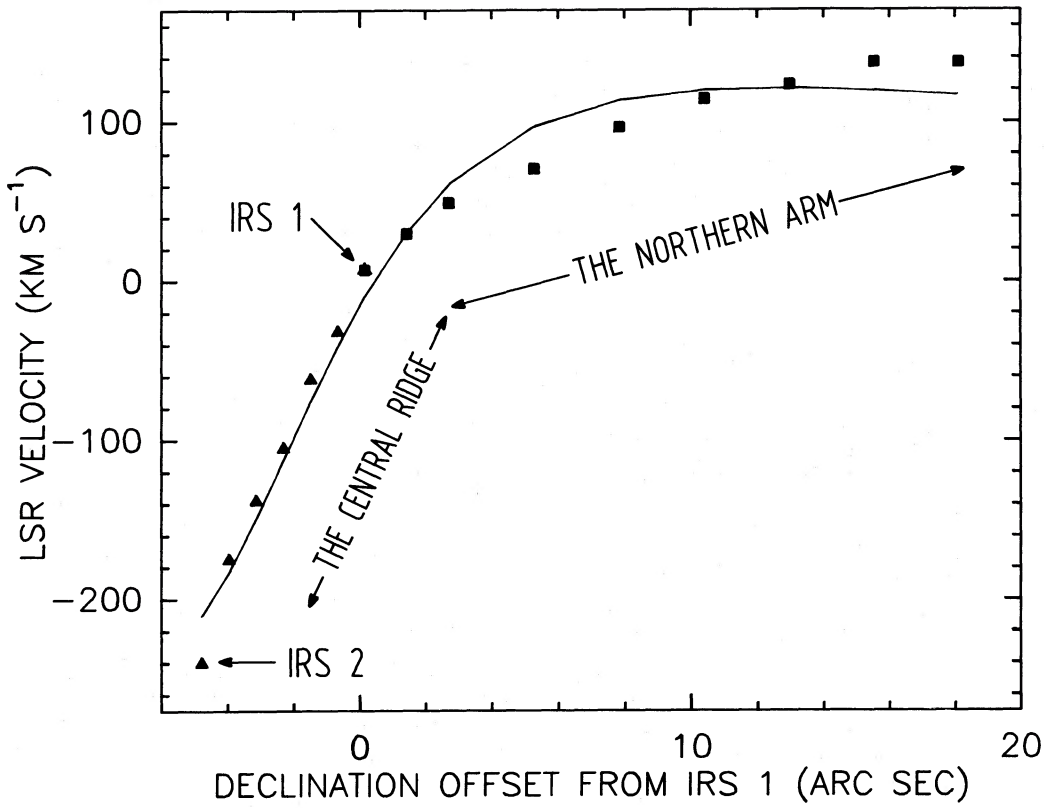


FIG. 9.—Velocities along the extended northern arm vs. declination offset from IRS 1. The squares show the 3'' resolution data from Paper I, and the triangles the 1''.5 data from this work.

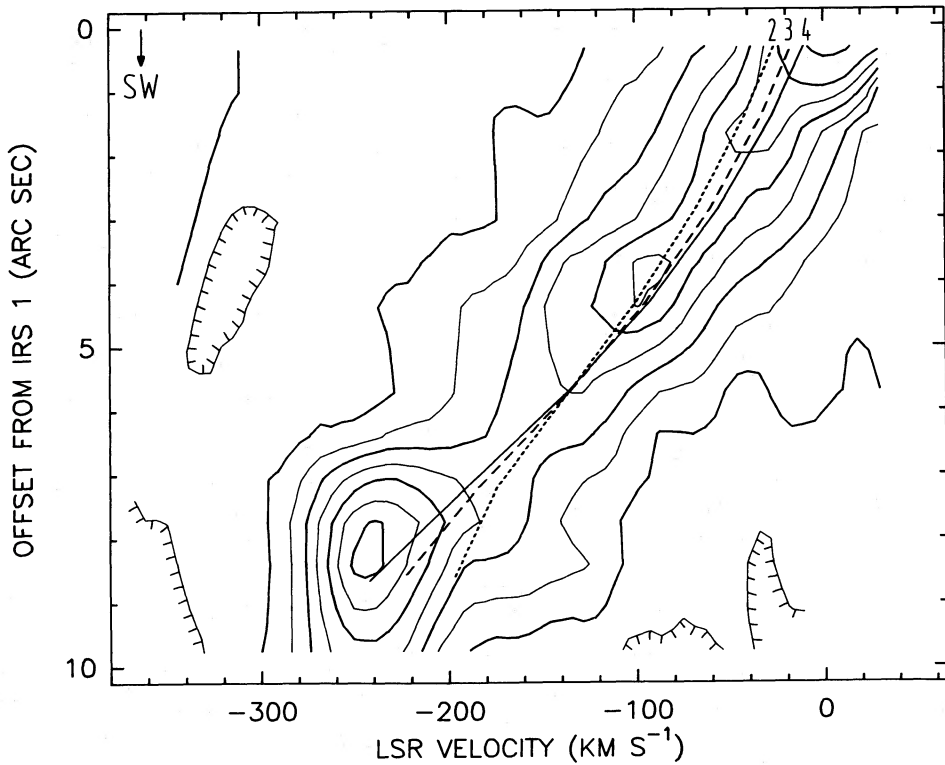


FIG. 10.—Parabolic orbit fits to the position velocity diagram along the central ridge. The curves shown are for central masses of 4, 3, and $2 \times 10^6 M_{\odot}$ located at the position of Sgr A*.

bolic orbits, elliptical and hyperbolic orbits yielded fits of equal quality. For a good fit with any Keplerian orbit, a central mass greater than $2.7 \times 10^6 M_\odot$, and $r_{\min} \sim 0.3$ pc are necessary. Because of the high-velocity gradients seen along this feature, only stellar clusters with $M_{1.7} > 15 \times 10^6 M_\odot$ allowed good fits.

c) Summary of Orbit Fitting Results

Together with the results of Paper I, the above results indicate that the velocities seen along most of the filaments in the central 2 pc are consistent with the filaments representing orbits of gas about the center. It is possible to fit orbits to both the position and velocity of the western arc and the northern arm (Paper I), and to the eastern arm and the central ridge (this paper). Although the extended northern arm could not be fitted well with a single orbit because of discontinuities in the orientation and velocity gradient at IRS 1, its general features can be reproduced, and the sections north and south of IRS 1 can be fitted well separately. However, it should be noted that along certain sections of the northern and eastern arms more than one velocity component is present, and hence the correct velocity component to associate with the filament is not always unambiguous.

Assuming that the correct velocity components have been followed along the filaments, the results give estimates of the masses within the orbits of the four features. The results for the central mass and stellar cluster cases are summarized in Table 1. The best founded of the entries is the mass estimate for the western arc from Paper I, as its near circular orbit allows a simple and direct mass determination. Furthermore, since this gas feature is probably on the inner surface of the surrounding molecular disk and has similar velocities, it has probably not been much affected by magnetic fields. Regarding the eastern arm, only the estimate based on the entire arm is entered: the high-velocity section alone is not very definitive, but is consistent with the mass estimate from the western arc.

The stellar cluster results indicate that, except for the high-velocity section of the eastern arm alone, all of the inner filaments require a stellar cluster at least twice as massive as that required by the western arc. A general reason for this is that because the enclosed mass decreases with radius in the stellar cluster, an orbit of a given angular momentum has much less curvature near the origin in the stellar cluster case than in the Keplerian case. This can be seen in Figure 11, which compares the shapes of an elliptical orbit about a central mass with one radial cycle of a stellar cluster orbit with similar r_{\min} , r_{\max} , and angular momentum. Since the stellar cluster orbit has much less curvature near the origin, a correspondingly lower radial velocity gradient on the sky is implied.

The orbits have also allowed estimates of the location of the

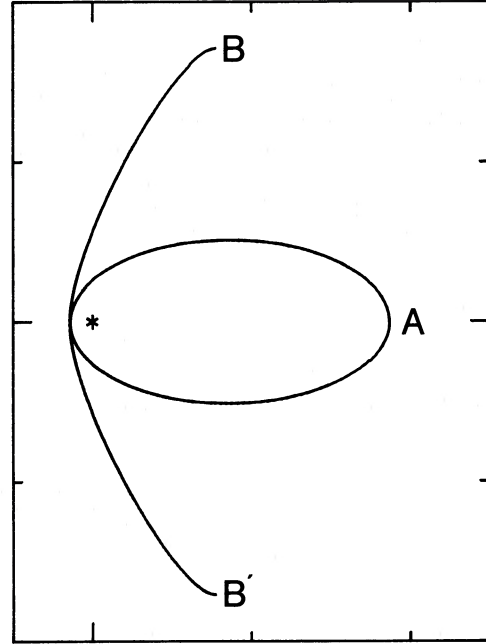


FIG. 11.—Comparison of orbits of similar size and angular momentum about a point mass (A) and in a stellar cluster (BB'). Orbit A is an elliptical orbit about a point mass of $4 \times 10^6 M_\odot$. Orbit BB' shows one full radial oscillation of an orbit in a stellar cluster with $M_{1.7} = 10^7 M_\odot$. The orbit is not closed but precesses around the center. The tick marks on the axes are 1.0 pc apart, and both orbits have $r_{\min} = 0.15$ pc and $r_{\max} = 1.9$ pc. The angular momenta are $67 \text{ km s}^{-1} \text{ pc}$ for the Keplerian orbit and $50 \text{ km s}^{-1} \text{ pc}$ for the stellar cluster orbit.

gravitational center. Based on the northern arm (Paper I), the best center is $\sim 2''$ E and $1''$ N of Sgr A*, while the eastern arm suggests a center $3''$ E and $2''$ S of Sgr A*. The two locations are consistent within the estimated accuracy ($\sim 3''$), but the declination is not well constrained. Thus, the kinematic origin shows a preference for a location $\sim 2''$ – $3''$ east of Sgr A*, or near the right ascension of IRS 16 NE (Forrest, Pipher, and Stein 1986). However, no source can be positively identified with the kinematic center.

VI. THE MASS DISTRIBUTION

Although the assumption that the filaments represent gravitationally dominated orbits is not unique, it has been shown to be a viable model, and so the mass distribution which is implied is now explored. Figure 12 shows the $[\text{Ne II}]$ kinematic mass estimates (located at the orbital r_{\min}), together with other mass estimates relating to the central 10 pc. The hatched area is derived from the kinematics of the molecular disk (Serabyn *et al.* 1986; Güsten *et al.* 1987), and the slope of the dashed line is from the $2 \mu\text{m}$ flux distribution from the central stellar cluster (Becklin and Neugebauer 1968). Because of an uncertain M/L ratio, the stellar data have been normalized to the $[\text{Ne II}]$ point at 1.7 pc. Recent observations of six individual stars (Sellgren *et al.* 1987) are consistent with these mass estimates.

Although beyond ~ 2 pc the kinematic and stellar mass estimates agree, the kinematic data at smaller radii suggest, as in Paper I, a mass distribution more centrally concentrated than the apparent distribution of the stellar cluster. This results basically from the difficulty in explaining the orbits of both the western arc (orbital velocity 110 km s^{-1} at 1.7 pc) and the

TABLE 1
MASS ESTIMATES FOR $R_0 = 10 \text{ kpc}^a$

	$M_{\text{point}}(10^6 M_\odot)$	$M_{1.7}(10^6 M_\odot)$	$r_{\min}(\text{pc})$
Western arc	4.7	4.7	1.7
Northern arm	> 3.0	> 11	0.5
Central ridge	> 2.7	> 15	0.3
Eastern arm ^b	> 2.0	> 10	0.2

^a The masses and radii scale linearly with R_0 , the distance to the Galactic center.

^b Inclusion of only the "high-velocity section" of the eastern arm (see text) gives a mass estimate consistent with that of the western arc.

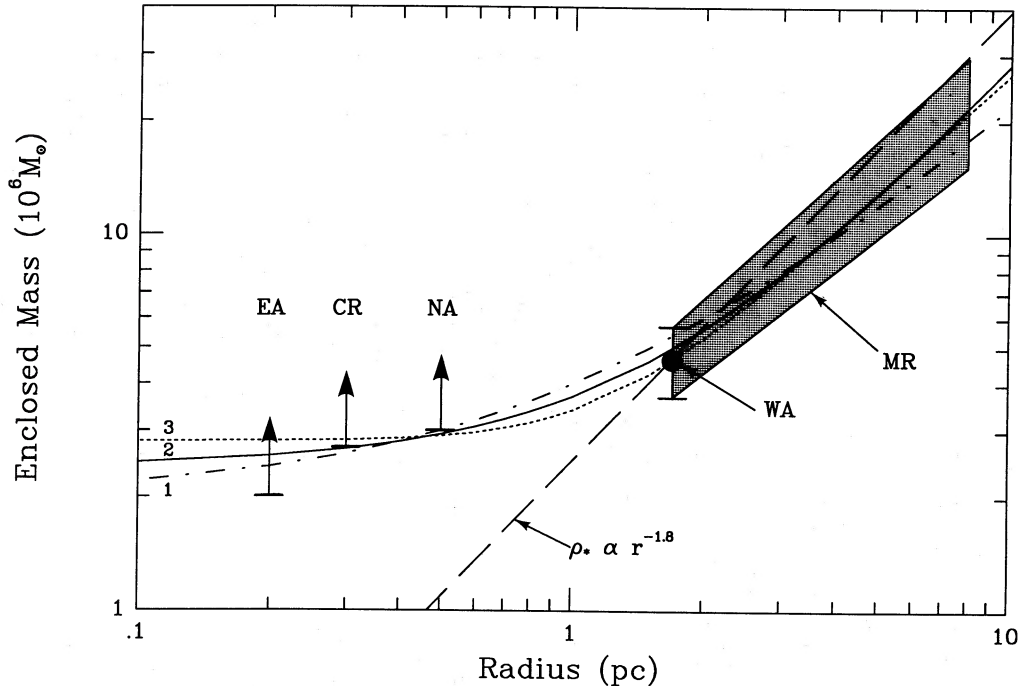


FIG. 12.—Kinematic mass estimates in the central 10 pc of our Galaxy. The hatched area (MD) is derived from the kinematics of the molecular disk at $r > 2$ pc (Serabyn *et al.* 1986; Güsten *et al.* 1987), and the four points and limits refer to the [Ne II] estimates listed in Table 1 (EA = eastern arm, CR = central ridge, NA = northern arm, WA = western arc). The dashed line gives the stellar mass estimate of Becklin and Neugebauer (1968), scaled to $M/L = 0.9$. The model curves show the mass distributions resulting from combining a point mass with the following stellar clusters: (1) $\rho \propto r^{-2}$, (2) $\rho \propto r^{-1.7}$, (3) isothermal King model with $r_c = 1$ pc.

inner filaments (e.g., the central ridge, with a terminal velocity of -260 km s^{-1} at $r \sim 0.3$ pc) with only a stellar cluster. The apparent concentration of mass toward the center can be attributed to a stellar cluster alone only if the cluster has a density which increases much more steeply inside a radius of 2 pc than the $r^{-1.7}$ rate deduced from the $2 \mu\text{m}$ stellar radiation. Such could be the case if, for example, the stellar distribution includes a substantial component of stars with high mass and low luminosity. This seems unlikely, and hence, in the following, mass models which include a massive central object are considered.

Figure 12 shows three possible models. The first consists of a singular isothermal stellar cluster of mass $M_*(r_{\text{pc}}) = 2M_6 r_{\text{pc}}$, in combination with a central point mass of $2M_6$, where r_{pc} is the radius in pc, and $M_6 = 10^6 M_\odot$. Although this type of model gives an acceptable fit to the data (model 1 in Fig. 12), the model slope at large radii is significantly shallower than the average slope of the trapezoidal area. To steepen the slope, either the power law describing the stellar distribution can be raised, or the mass of stars in the central region can be lowered by the inclusion of a lower density core in the stellar distribution. The first approach is shown as model 2, in which the stellar mass is given by $M_*(r_{\text{pc}}) = 1.3M_6 r_{\text{pc}}^{1.3}$, a radial dependence consistent with the stellar measurements (Allen, Hyland, and Jones 1983). To make up for the consequent lower stellar mass in the central pc, a somewhat higher point mass of $2.4M_6$ was needed, but good fits to the data result. The alternative of a core in the stellar distribution was investigated by combining a point mass of $2.8M_6$ with an isothermal King model stellar distribution. As model 3 shows, a core radius of 1 pc in the

King model allows a good fit. Thus, both of the latter models fit the kinematic data at all radii quite well, and a flat mass distribution at small radii is compatible with the rapidly rising mass distribution outside of 2 pc. Both types of model give a similar value for the central mass, $\sim 2.5 \times 10^6 M_\odot$ (or $\sim 2 \times 10^6 M_\odot$ for $R_0 = 8.5$ kpc).

Since the mass distributions for models 2 and 3 are so similar, it is not possible to discriminate between them on the basis of the kinematic measurements. Thus the size of the core in the stellar distribution may better be determined from observations of the stellar cluster. Although earlier observations tended to support a small core radius (≤ 0.05 pc; Bailey 1980), a core radius as large as 1 pc has recently been proposed (Rieke and Lebofsky 1987), and may be a viable possibility.

On the other hand, a completely flat core is not expected in the presence of a massive central object. Calculations of the equilibrium distribution of stars around a black hole predict a stellar distribution which has a central cusp with $\rho \propto r^{-1.75}$ at small radii, and a normal King model distribution outside of the cusp (e.g., Marchant and Shapiro 1979). Since such a model would lie between our models 2 and 3, it could also provide a good fit to the kinematic observations. Again, based on the kinematic data, it is not possible to discriminate between such a model and models 2 and 3.

In summary, the combination of the central point mass and a roughly isothermal stellar cluster allows good fits to the kinematic mass distribution throughout the inner 10 pc of the Galaxy. However, because at smaller radii the point mass dominates the ensuing mass distribution, the stellar distribution in the inner parsec is not well constrained. Thus, in the

inner parsec, the present kinematic data cannot be used to distinguish between the presence or absence of either a central core or cusp in the stellar distribution.

We would like to thank R. Güsten and D. M. Watson for

helpful discussions, K. Y. Lo for providing the radio continuum map, and the staff of the IRTF for assistance with the observations. E. Serabyn was partially supported by NSF grant AST-8512055 and NASA grant 05-003-272, and J. H. Lacy by NSF grant AST-8502401.

REFERENCES

- Aitken, D. K., Roche, P. F., Bailey, J. A., Briggs, G. P., Hough, J. H., and Thomas, J. A. 1986, *M.N.R.A.S.*, **218**, 363.
- Allen, D. A., Hyland, A. R., and Jones, T. J. 1983, *M.N.R.A.S.*, **294**, 1145.
- Allen, D. A., and Sanders, R. H. 1986, *Nature*, **319**, 191.
- Backer, D. C., and Sramek, R. A. 1982, *Ap. J.*, **260**, 512.
- . 1987, in *AIP Conf. Proc. 155, The Galactic Center*, ed. D. C. Backer, p. 163.
- Bailey, M. E. 1980, *M.N.R.A.S.*, **190**, 217.
- Bally, J., Stark, A. A., Wilson, R. W., and Henkel, C. 1987, *Ap. J. (Suppl.)*, **65**, 13.
- Becklin, E. E., Gatley, I., and Werner, M. W. 1982, *Ap. J.*, **258**, 135.
- Becklin, E. E., and Neugebauer, G. 1968, *Ap. J.*, **151**, 145.
- Becklin, E. E., and Neugebauer, G. 1975, *Ap. J. (Letters)*, **220**, L71.
- Brown, R. L. 1982, *Ap. J.*, **262**, 110.
- Brown, R. L., and Johnston, K. J. 1983, *Ap. J. (Letters)*, **268**, L85.
- Brown, R. L., and Liszt, H. S. 1984, *Ann. Rev. Astr. Ap.*, **22**, 223.
- Ekers, R. D., van Gorkom, J. H., Schwartz, U. J., and Goss, W. M. 1983, *Astr. Ap.*, **122**, 143.
- Forrest, W. J., Pipher, J. L., and Stein, W. A. 1986, *Ap. J. (Letters)*, **301**, L49.
- Forrest, W. J., Shure, M. A., Pipher, J. L., and Woodward, C. E. 1987, in *AIP Conf. Proc. 155, The Galactic Center*, ed. D. C. Backer, p. 153.
- Gatley, I., Jones, T. J., Hyland, A. R., Wade, R., Geballe, T. R., and Krisciunas, K. 1986, *M.N.R.A.S.*, **222**, 299.
- Geballe, T. R. 1987, in *AIP Conf. Proc. 155, The Galactic Center*, ed. D. C. Backer, p. 39.
- Geballe, T. R., Wade, R., Krisciunas, K., Gatley, I., and Bird, M. C. 1987, *Ap. J.*, **320**, 562.
- Geballe, T. R., Krisciunas, K., Lee, T. J., Gatley, I., Wade, R., Duncan, W. D., Garden, R., and Becklin, E. E. 1984, *Ap. J.*, **284**, 118.
- Genzel, R., and Townes, C. H. 1987, *Ann. Rev. Astr. Ap.*, **25**, 377.
- Genzel, R., Watson, D. M., Crawford, M. K., and Townes, C. H. 1985, *Ap. J.*, **297**, 766.
- Gezari, D. Y., Tresch-Fienberg, R., Fazio, G. G., Hoffmann, W. F., Gatley, I., Lamb, G., Shu, P., and McCreight, C. 1985, *Ap. J.*, **299**, 1007.
- Güsten, R., Genzel, R., Wright, M. C. H., Jaffe, D. T., Stutzki, J., and Harris, A. I. 1987, *Ap. J.*, **318**, 124.
- Hall, D. N. B., Kleinmann, S. G., and Scoville, N. Z. 1982, *Ap. J. (Letters)*, **262**, L53.
- Harris, A. I., Jaffe, D. T., Silber, M., and Genzel, R. 1985, *Ap. J. (Letters)*, **294**, L93.
- Heyvaerts, J., Norman, C., and Pudritz, R. E. 1987, preprint.
- Ishiguro, M., Fomalont, E., Morita, K.-I., Kasuga, T., Kanzawa, T., Iwashita, H., Kawabe, R., Kobayashi, H., and Okumura, S. 1987, preprint.
- Krisciunas, K., Geballe, T. R., and Wade, R. 1985, *Bull. A.A.S.*, **16**, 980.
- Lacy, J. H. 1979, Ph.D. thesis, University of California, Berkeley.
- Lacy, J. H., Bass, F., Townes, C. H., and Geballe, T. R. 1979, *Ap. J. (Letters)*, **227**, L17.
- Lacy, J. H., Lester, D. F., and Arens, J. F. 1987, in *AIP Conf. Proc. 155, The Galactic Center*, ed. D. C. Backer, p. 142.
- Lacy, J. H., Townes, C. H., Geballe, T. R., and Hollenbach, D. J. 1980, *Ap. J.*, **241**, 132.
- Lacy, J. H., Townes, C. H., and Hollenbach, D. J. 1982, *Ap. J.*, **262**, 120.
- Liszt, H. S., Burton, W. B., and van der Hulst, J. M. 1985, *Astr. Ap.*, **142**, 237.
- Lo, K. Y. 1986, *Science*, **233**, 1394.
- Lo, K. Y., Backer, D. C., Ekers, R. D., Kellermann, D. I., Reid, M., and Moran, J. M. 1985, *Nature*, **315**, 124.
- Lo, K. Y., and Claussen, M. J. 1983, *Nature*, **306**, 647.
- Lo, K. Y., Cohen, M. H., Readhead, A. S. C., and Backer, D. C. 1981, *Ap. J.*, **249**, 504.
- Lugten, J. B., Genzel, R., Crawford, M. K., and Townes, C. H. 1986, *Ap. J.*, **306**, 691.
- Marchant, A. B., and Shapiro, S. L. 1979, *Ap. J.*, **234**, 317.
- McCray, R., and Snow, T. P. 1979, *Ann. Rev. Astr. Ap.*, **17**, 213.
- Mezger, P. G., and Wink, J. E. 1986, *Astr. Ap.*, **157**, 252.
- Morris, M., and Yusef-Zadeh, F. 1987, in *AIP Conf. Proc. 155, The Galactic Center*, ed. D. C. Backer, p. 127.
- Petroff, M. D., and Stapelbroek, M. G., *Blocked Impurity Band Detectors*, United States Patent Number 4,568,960, filed October 23, 1980, issued February 4, 1986.
- Quinn, P. J., and Sussman, G. J. 1985, *Ap. J.*, **288**, 377.
- Rieke, G. H., and Lebofsky, M. J. 1987, in *AIP Conf. Proc. 155, The Galactic Center*, ed. D. C. Backer, p. 91.
- Sandqvist, A., Wooten, A., and Loren, R. B. 1985, *Astr. Ap.*, **152**, L25.
- Sellgren, K., Hall, D. N. B., Kleinmann, S. G., and Scoville, N. Z. 1987, *Ap. J.*, **317**, 881.
- Serabyn, E. 1984, Ph.D. thesis, University of California, Berkeley.
- Serabyn, E., and Güsten, R. 1987, *Astr. Ap.*, **184**, 133.
- Serabyn, E., Güsten, R., Walmsley, C. M., Wink, J. E., and Zylka, R. 1986, *Astr. Ap.*, **169**, 85.
- Serabyn, E., and Lacy, J. H. 1985, *Ap. J.*, **293**, 445 (Paper I).
- Storey, J. W. V., and Allen, D. A. 1983, *M.N.R.A.S.*, **204**, 1153.
- van Gorkom, J. H., Schwarz, U. J., and Bregman, J. D. 1983, in *IAU Symposium 106, The Milky Way Galaxy*, ed. H. van Woerden, W. B. Burton, and R. J. Allen (Dordrecht: Reidel), p. 371.
- Wollman, E. R., Geballe, T. R., Lacy, J. H., Townes, C. H., and Rank, D. M. 1976, *Ap. J. (Letters)*, **205**, L5.
- . 1977, *Ap. J. (Letters)*, **218**, L103.
- Wright, M. C. H., Genzel, R., Güsten, R., and Jaffe, D. T. 1987, in *AIP Conf. Proc. 155, The Galactic Center*, ed. D. C. Backer, p. 133.
- Yusef-Zadeh, F., and Morris, M. 1987, *Ap. J.*, **320**, 545.

R. BHARAT: Rockwell International Science Center, 3370 Miraloma Avenue, Anaheim, CA 92803

J. H. LACY: University of Texas, Department of Astronomy, Austin, TX 78712

E. SERABYN: California Institute of Technology, Department of Physics 320-46, Pasadena, CA 91125

C. H. TOWNES: University of California, Department of Physics, Berkeley, CA 94720